Research Square

Preprints are preliminary reports that have not undergone peer review.
They should not be considered conclusive, used to inform clinical practice,
or referenced by the media as validated information.

Intelligent Optimization of Wind Farm Layout Under Wind Turbine Wake Effect Based on Deep Learning and Fluid Dynamics

Shujie Liu
PowerChina Huadong Engineering Coa. Ltd.
Shengqiao Chen
Huazhong University of Science and Technology
Bo Xiang
594789866@163.com

Huazhong University of Science and Technology

Research Article

Keywords: Wind farm layout optimization, Turbine wake effect, Physical Information Neural Network, Graph Attention Network, Deep Reinforcement Learning

Posted Date: September 11th, 2026

DOI: https://doi.org/10.21203/rs.3.rs-9988328/v1

License: This work is licensed under a Creative Commons Attribution 4.0 International License.
Read Full License

Additional Declarations: No competing interests reported.

Intelligent Optimization of Wind Farm Layout Under Wind Turbine Wake Effect Based on Deep Learning and Fluid Dynamics

Shujie Liu[1], Shengqiao Chen[2], Bo Xiang[2]*

[1]*PowerChina Huadong Engineering Coa. Ltd., Hangzhou 311122, China*

[2]*School of Civil and Hydraulic Engineering, Huazhong University of Science and Technology, Wuhan 430074, China*

Corresponding Author: Bo Xiang

Email: 59478986@163.com

Abstract

Large-scale wind farm expansion suffers from wake losses of 10% – 20%, which significantly erode annual energy production. Existing approaches for wake modeling and layout optimization face trade-offs between accuracy, efficiency, and robustness due to simplified analytical models, costly CFD simulations, lack of physical consistency in data-driven methods, and high-dimensional heuristic optimization bottlenecks. This paper proposes an end-to-end collaborative framework that integrates deep learning with fluid dynamics. The framework jointly trains three modules: a physics-informed neural network that embeds RANS momentum and continuity equation residuals as soft constraints in the loss function to enforce conservation laws in sparse data regions; a graph attention network that represents turbines as nodes and upstream-downstream couplings as directed edge features, learning coupling weights via multi-head attention; and a deep reinforcement learning layer that formalizes layout selection as a Markov decision process, driving PPO training with a multi-objective reward combining power generation and wake uniformity. On an 80-turbine benchmark equivalent to Horns Rev I, the method reduces flow field prediction RMSE by 67% versus Bastankhah-Gauss and by 49% versus a CNN-only model, achieves an R^2 of 0.97, and compresses single-condition inference time to 41 ms. For layout optimization, AEP increases by 5.7%, wake loss decreases from 11.4% to 6.5%, and consistent improvements of 4.4% – 5.9% are observed across five wind condition categories. The approach scales to 200 turbines while maintaining hundred-millisecond-level inference. This study delivers a reusable methodology chain for intelligent large-scale onshore and offshore wind farm layout optimization, balancing accuracy, efficiency, and robustness.

Keywords: Wind farm layout optimization, Turbine wake effect, Physical Information Neural Network, Graph Attention Network, Deep Reinforcement Learning

1 Introduction

Driven by the transformation of energy structure, wind energy is growing at an unprecedented speed as the core component of the power system. The cumulative installed capacity of global wind power has exceeded 1100 GW and reached 1136 GW by the end of 2024. The installed capacity of offshore wind power has exceeded 15 MW, while onshore wind farms continue to evolve towards higher density and larger scale iteration [1]. However, the wake effect in the operation of the wind turbine cluster is becoming a key technical bottleneck eroding the annual power generation of the wind farm: after the upstream wind turbine extracts kinetic energy from the atmosphere, the inflow velocity faced by the downstream wind turbine will suffer a loss of 30%-50%, and the turbulence

intensity will increase significantly, which will then drag down the overall power generation efficiency and unit fatigue life [2]. A number of studies have shown that the internal wake loss of large-scale wind farms is generally in the range of 10% -20%, which may even be higher in the dense layout or the alignment of the dominant wind direction, directly affecting the levelized kilowatt hour cost and grid connected benefits [3,4]. How to internalize the wake coupling effect into the layout decision in the wind farm planning stage has become the common concern of the engineering and academic circles.

The traditional wind farm layout optimization path has long been around the "analytical wake model+heuristic optimization": Jensen, bastankhah port é -agel and other analytical models abstract the wake as a top hat or Gaussian velocity loss, and then use genetic algorithm, particle swarm optimization and other heuristic strategies to search for the optimal layout in the discrete configuration space [5]. This paradigm is effective for small-scale wind farms, but in the face of large-scale, complex terrain and variable wind conditions, the simplified assumptions of the analytical model are difficult to describe the turbulence superposition and wake deflection under the real multi machine coupling, and the high fidelity CFD simulation cannot be directly embedded into the optimization cycle due to the computational cost of several hours under single working condition [6]. Deep learning has been involved in this field in recent years. Convolutional networks and graphical neural networks have been used as flow field proxies or power predictors, making a breakthrough in the trade-off between accuracy and speed [7, 8]. However, there are two shortcomings in the existing research: one is that the agent model and the optimizer are independent, and the flow field predictor only serves for a single evaluation, and does not return the graph structure information of multi machine spatial coupling to the optimization decision; Second, the generalization ability of the optimization algorithm for high-dimensional complex wind conditions is limited, and it is easy to fall into local optimization in real multi wind and multi wind scenarios.

Around the above short board, this study proposes an end-to-end collaborative framework combining deep learning and fluid dynamics, tightly coupling the three-tier modules of "physical information constrained wake field proxy+multi machine coupling representation of graph attention+layout strategy optimization of deep reinforcement learning". In the wake modeling layer, the residual of RANS momentum equation and continuity equation are written into the network loss as soft constraints, so that the proxy model also obeys the conservation law in the data sparse area; In the multi machine coupling layer, the graph attention mechanism is used to learn the directional coupling weights between upstream and downstream fans, which overcomes the simplification of neighborhood structure in the existing data-driven model; In the layout optimization layer, the selection of fan points is formalized as a Markov decision process, and the PPO is used to learn the global optimal layout strategy under the guidance of multi-objective rewards. The three-tier module realizes end-to-end joint training by sharing intermediate representations, which makes physical consistency, spatial structure perception and strategy level search mutually enhanced. The main innovations of this study can be summarized into three aspects: a lightweight wake field proxy constrained by physical information is proposed, which can reduce the reasoning time to sub second level while preserving the accuracy of Les level; Construct the graph attention driven multi machine coupling representation, and take the spatial graph structure as a part of the reinforcement learning state space for the first time; Realize end-to-end strategy level layout optimization, so that layout generation is no longer dependent on external heuristic search and is directly generated by the strategy network [9].

2 Related work

2.1 Research status of fan wake modeling

Wake modeling is the physical basis of wind farm design and operation decision, which can be

roughly divided into three paths: analytical model, CFD high fidelity simulation and data-driven agent. In terms of the analytical model, bastankhah et al. Promoted the analytical expression of the coupling between the far-field deflection of the wake and the turbulence intensity on the basis of the Gaussian profile, so that the wake direction under the speed loss and yaw control can be described by the engineering formula at the same time [9]. Yousif et al. Introduced physics guided deep learning into the generation of turbulent inflow conditions, showing the improvement of the accuracy of inflow field reconstruction by integrating the conservation law soft constraint into network training [10]. Duth é et al. Built a multi fidelity framework based on graph neural network and transfer learning on the data-driven engineering platform of Cambridge, coupled high and low fidelity data under the unified graph structure, and provided a transferable paradigm for the proxy modeling of wind farm flow field and load [11]. Kim et al. Carried out unsupervised depth learning for super-resolution reconstruction of turbulent flow field, suggesting a feasible path for low resolution samples to restore high-resolution flow field through depth network [12]. The above work reveals that the pure analytical formula is difficult to capture the far-field wake deflection, wind direction coupling and turbulence intensity evolution under real working conditions, and the accuracy attenuation is obvious under dense layout and multidirectional wind conditions, which cannot directly support thousands of working condition evaluations in the optimization process.

The CFD high fidelity path, represented by LES and RANS, can accurately describe the spatio-temporal evolution of wake at the grid scale. Locarcio et al. Systematically summarized the advantages and bottlenecks of LES in wind turbine wake simulation, and pointed out that the solution time of single condition of large-scale wind farms is still on the order of hours or even days, which is difficult to adapt to the optimization internal cycle [13]. van der Laan et al. proposed a steady-state RANS inflow model based on a constant Brunt–Väisälä frequency for neutral and stable atmospheric boundary layers and applied it to wind turbine wake simulations, achieving good agreement with LES in single-wake velocity deficit prediction, but pointing out that the model still suffers from numerical convergence issues in shallow boundary-layer and large-scale wind farm scenarios [14]. Santoni et al. proposed an autoencoder convolutional neural network with U-Net skipped connections fine-tuned by LES data to augment analytical engineering wake models, reducing the prediction error from 20% of the Gauss Curl Hybrid model to less than 5% while maintaining the computational cost of the analytical model, but the framework still relies on a large amount of high-fidelity training data and the inherent contradiction between "high fidelity is high time consuming" has not yet been completely overcome [15]. Faroughi et al. Systematically reviewed the application of physical guidance/physical information/physical coding neural network in fluid mechanics, providing a methodological basis for how the agent model absorbs physical knowledge [16]. In general, CFD high fidelity is irreplaceable in accuracy, but its computational power cost in single working condition determines that it can only be used as the training data source of agent model, rather than the environment simulator directly called by the optimizer.

2.2 Progress of deep learning in wake field prediction and multi machine coupling characterization

The data-driven agent model attempts to approximate the input-output mapping of les/rans with neural network, so as to reduce the reasoning to less than seconds while maintaining high fidelity. Cai et al. Systematically reviewed the application of physical information neural network in fluid mechanics, and pointed out that PDE soft constraint can significantly improve the generalization ability of the network in the data sparse area [17]. Cuomo et al. Reviewed the research context of scientific machine learning and pinn on a broader scale, and discussed the open problems of multiple loss term weight balance, convergence stability and boundary condition embedding [18]. Ashwin renganathan et al. Introduced probabilistic machine learning into wake modeling and characterized the prediction uncertainty through Bayesian neural network, which alleviated the overconfidence problem of point estimation proxy model under extrapolation conditions [19]. Ye et al.

Systematically compared ANN, CNN, GNN, attention and other data-driven wake models in their latest review, and pointed out that physical embedding and graph structure coupling are the two main lines of current development [20]. However, there is a general lack of physical consistency in the pure data-driven model in the data sparse area or extrapolation condition, and the training stability of the network, the weight balance of loss items, and the scale matching of PDE residuals have not yet formed a mature scheme.

Graph neural network and attention mechanism encode the natural spatial structure of wind farms into network representation, which is becoming a new main line of multi machine coupling modeling. Zehtabiyan et al. Introduced graph convolution into wind farm flow field reconstruction, and verified the advantages of graph structure over regular grid in multi machine coupling characterization [21]. Peng et al. constructed a spatio-temporal wind propagation graph in Renewable Energy and used graph attention network for wind power ramp event prediction, characterizing the difference of inter-station coupling strength under different wind propagation conditions through adaptive learning of node importance [22]. Romero et al. Proposed that the deep volume integration layer codec network can predict the wake loss of the wind farm end-to-end, and model the power output under the multi machine coupling as a coherent regression task while preserving the convolution spatial sensing ability [23]. Song et al. introduced a diffusion model into a three-dimensional dynamic wake prediction framework for multiple turbine operating states, demonstrating the potential of generative diffusion models to mitigate prediction over-smoothing and capture transient wake characteristics under varying inflow and turbine control conditions [24]. The above work has jointly promoted the paradigm shift of "agent model from single point regression to full field modeling", but it is still mainly used for power prediction, and the graph structure representation has not been reversed into the layout optimization decision, resulting in a structural separation between the agent model and the optimizer.

2.3 Research on intelligent optimization algorithm of wind farm layout

Genetic algorithm, particle swarm optimization, simulated annealing and other heuristic strategies have been the mainstream of wind farm layout optimization for a long time. Bouchekara et al. Proposed a multi-objective heuristic algorithm for real wind farm expansion, and gave Pareto solution set between wake loss and construction cost [25]. Malisani et al. formulated the offshore wind farm layout optimization with grid-alignment constraints as a mixed-integer nonlinear programming problem in Wind Energy Science, and developed a heuristic-based solving algorithm coupling angle search-space reduction with local search, verifying the solution quality and computational efficiency on the IEA Wind Task 37 benchmark [26]. Liew et al. Proposed model free reinforcement learning based on recursive least squares for wind farm closed-loop control, and proved that strategy learning without accurate wake model can also reduce wake loss at the control level, providing practical evidence for the paradigm shift of optimization algorithm [27]. Traditional heuristics can quickly give feasible solutions in small-scale and single wind conditions, but in the face of the high-dimensional configuration space and variable wind conditions of hundreds of fans, the search space expands exponentially, and the heuristic strategy is easy to fall into local optimization.

Reinforcement learning has been involved in this field in recent years, modeling "layout generation" as a sequential decision-making process, and replacing heuristic random search with strategy network. Yu and Lu developed a reinforcement learning-based multi-objective differential evolution algorithm for wind farm layout optimization in Energy, employing reinforcement learning to coordinate the parameters of differential evolution and balance global and local search, verifying the convergence advantage of strategy-level adaptive control over fixed-parameter heuristics under multi-objective trade-offs between power generation and farm cost [28]. Hu et al. coupled CFD-based wind resource assessment with an improved genetic algorithm and particle swarm

optimization (IGA-PSO) in Energy for wind farm layout optimization in complex terrain, integrating measured wind data with CFD simulation through inverse distance weighting, and achieving better annual energy production on the irregular Qianjiang complex-terrain site under multiple wake and cost models [29]. Lin et al. Used Multi-Agent Reinforcement Learning on Frontiers in energy research to jointly consider the collaborative optimization of layout and active power scheduling, and pushed the optimization problem from single-layer layout to "layout operation" double-layer coupling [30]. On the whole, reinforcement learning has shown its potential to surpass heuristics at the optimization level, but the existing environmental simulators mostly rely on the low fidelity analytical model, resulting in the feedback signal of strategy learning being bound by the proxy accuracy, and there is still room for significant improvement in the physical rationality and robustness of the layout strategy. The close coupling of high-precision physical consensus agent and strategy level optimization, and the graphical structure representation of multi machine coupling as a part of the state space, is the key link that this research tries to complement, and also the starting point of the design of the method chain in the following chapter 3.

3 Experimental design

3.1 Overall research plan and technical route

Around the three-tier task of "wake field agent+multi machine coupling characterization+ layout strategy optimization", this study constructs an end-to-end collaborative method chain. The overall research scheme is carried out along the five links of "data generation - agent modeling - coupling characterization - Strategy Optimization - deployment evaluation". The front and back modules are mutually constrained by sharing intermediate representations, integrating the flexibility of data driving and the interpretability of fluid mechanics, as shown in Figure 1.

In the data generation section, the true values of the whole field velocity and turbulence intensity are generated by high fidelity Les simulation as the training labels of the downstream agent network; The physical information neural network (pinn) is embedded into the regression task of the wake velocity field in the agent modeling process, and the agent also maintains fluid conservation in the data sparse area through the RANS residual soft constraint; The directed coupling between multiple machines is encoded into the eigenvector of the inlet fan node by the graph attention network (GAT) in the coupling representation link; In strategy optimization, the global graph of GAT is embedded as the state feature of reinforcement learning, and PPO agent outputs the incremental adjustment action of fan point position; The deployment evaluation link evaluates the accuracy, efficiency and robustness of the system on a multi wind and multi-scale benchmark field, and compares it with the heuristic baseline. The above five rings realize end-to-end cooperation through two-stage training: first, the pinn-gat agent is pre trained on the LES data set, and then the agent parameters are fixed in the strategy training phase, and the action output is updated in reverse with PPO.

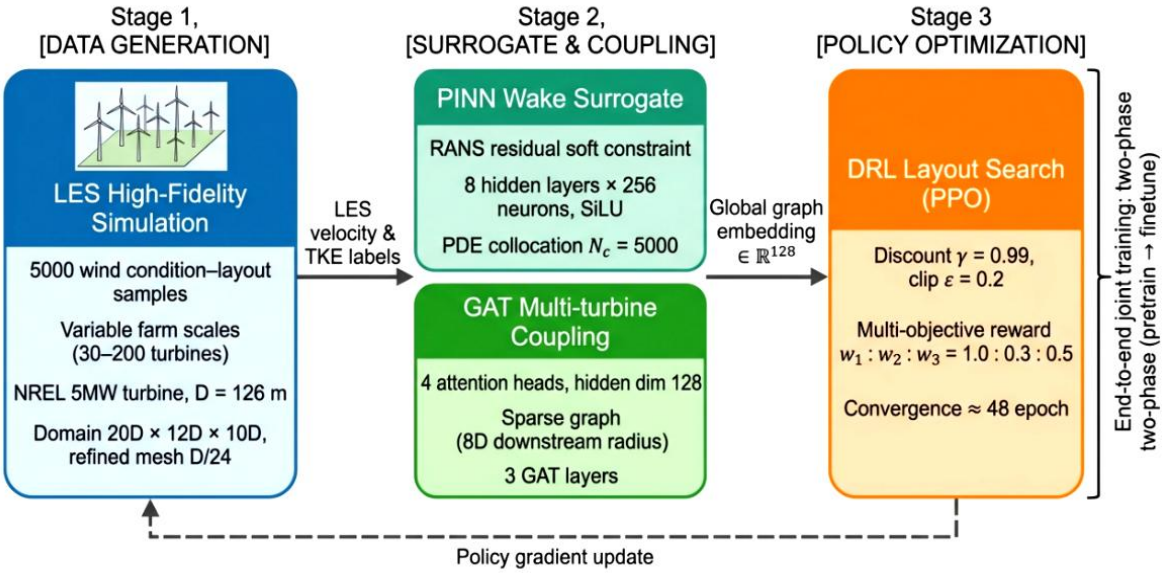


Figure 1 overall research framework and three-tier module data flow diagram

3.2 Construction of the Tailflow Field Agent Model with Physical Information Constraints

The Tailflow Field Agent Model (PINN) incorporates the residuals of the RANS momentum equation and the continuity equation as soft constraints into the network loss function. Its architecture features a fully connected encoding backbone supplemented with multi-scale residual blocks, which processes wind farm geometric coordinates and inflow conditions to produce a three-component velocity field and turbulent kinetic energy. The RANS momentum equation serves as the core constraint for time-average flow, as illustrated in Equation (1); the continuity equation governs mass conservation in incompressible flows, as shown in Equation (2); and the equivalent source term for the turbine thrust disk is presented in Equation (3).

$$\frac{\partial U_i}{\partial t} + U_j \frac{\partial U_i}{\partial x_j} = -\frac{1}{\rho}\frac{\partial P}{\partial x_i} + \frac{\partial}{\partial x_j}\left[\nu\left(\frac{\partial U_i}{\partial x_j} + \frac{\partial U_j}{\partial x_i}\right) - \overline{u_i' u_j'}\right] + f_i \tag{1}$$

$$\frac{\partial U_i}{\partial x_i} = 0 \tag{2}$$

$$f_i = -\frac{1}{2}\rho C_T A_R U_\infty^2 \delta(x - x_d) \tag{3}$$

In equation (1), U_i denotes the time-average velocity component, P represents pressure, ρ is air density, ν is kinematic viscosity, $\overline{u_i' u_j'}$ is the Reynolds stress tensor, and f_i is the equivalent source term for fan thrust. In Equation (3), C_T denotes the thrust coefficient, A_R represents the rotor swept area, U_∞ is the inlet velocity, and $\delta(x - x_d)$ denotes the Dirac function at the turbine location x_d. The PINN total loss combines the data fitting loss, the PDE residual loss, and the boundary condition loss in a weighted manner, as shown in Equation (4); the PDE residual loss is given by Equation (5).

$$\mathrm{L}_{\text{total}} = \lambda_{\text{data}}\mathrm{L}_{\text{data}} + \lambda_{\text{PDE}}\mathrm{L}_{\text{PDE}} + \lambda_{\text{BC}}\mathrm{L}_{\text{BC}} \tag{4}$$

$$L_{PDE} = \frac{1}{N_c}\sum_{n=1}^{N_c}\left|R_{NS}(x_n;\theta)\right|^2 \tag{5}$$

In equation (4), λ_{data}, λ_{PDE}, and λ_{BC} are the weight coefficients of the multiple loss terms, dynamically adjusted by an adaptive weight balancing strategy to mitigate scale mismatch among the loss terms; in equation (5), N_c denotes the number of sampling points, R_{NS} is the RANS equation residual operator, and θ represents the network's trainable parameters. The PINN network architecture employs an 8-layer fully connected encoding backbone, with each layer containing 256 neurons and the SiLU activation function. Its output is connected to multi-scale residual blocks to enhance the capture of wake gradient variations, as illustrated in Figure 2. During training, LES ground truth serves as the supervision signal for L_{data}, while 5,000 randomly sampled collocation points within the domain are used for L_{PDE}, and 1,000 boundary points are utilized for L_{BC}.

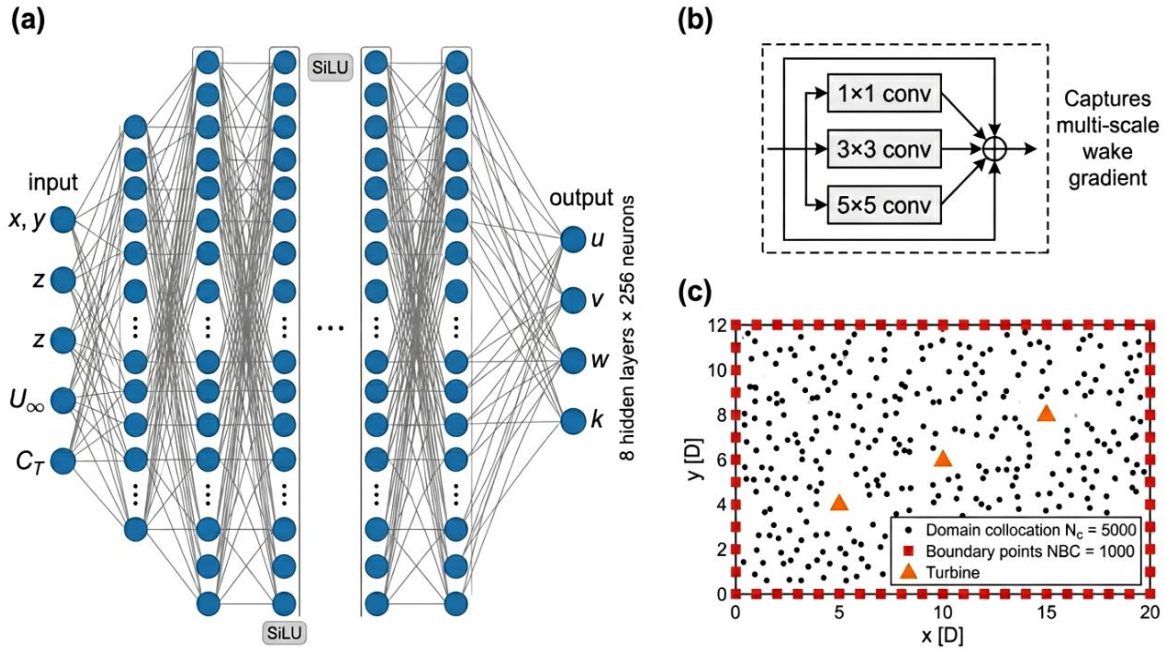


Figure 2 pinn proxy model architecture combination diagram

3.3 Multi-Turbine Wake Coupling Representation Based on Graph Attention Networks

Wake coupling in multi-turbine wind farms fundamentally involves the propagation of spatial graph structure information. This study treats each turbine as a node in the graph, with the geometric relationships between upstream and downstream turbines in wind direction projection serving as directed edges. The Graph Attention Network (GAT) learns adaptive weights for coupling intensity, condensing multi-turbine interaction information into node-level feature vectors. Initial node features include turbine position coordinates, hub height, rotor diameter, thrust coefficient, and local inflow velocity provided by PINN; edge features encode node distance, azimuth angle, wind direction projection, and upstream thrust influence factor, as shown in Equation (6).

$$e_{ij} = \phi_e\left(\| x_j - x_i \|, \cos\alpha_{ij}, U_\infty, C_{T,i}\right) \tag{6}$$

In Equation 6, e_{ij} represents the edge feature from node i to node j, $\| x_j - x_i \|$ denotes the distance between the nodes, α_{ij} is the angle between the wind direction and the connecting line, U_∞ is the inflow wind speed, $C_{T,i}$ is the upstream turbine thrust coefficient, and ϕ_e is a trainable

edge feature encoder implemented using a two-layer MLP. The GAT attention coefficient reflects node i's attention to its neighbor j, as shown in Equation (7); the node feature update rule aggregates the features of neighboring nodes weighted by attention scores, as illustrated in Equation (8).

$$\alpha_{ij} = \frac{\exp\left(\text{LeakyReLU}\left(a^{\cdot}\left[Wh_i \| Wh_j \| We_{ij}\right]\right)\right)}{\sum_{k\in \mathrm{N}_i} \exp\left(\text{LeakyReLU}\left(a^{\cdot}\left[Wh_i \| Wh_k \| We_{ik}\right]\right)\right)} \tag{7}$$

$$h_i^{(l+1)} = \sigma\left(\sum_{j\in \mathrm{N}_i} \alpha_{ij}^{(l)} W^{(l)} h_j^{(l)}\right) \tag{8}$$

In equations (7) and (8), h_i denotes the hidden feature of node i at layer l, W is the trainable linear transformation matrix, a is the trainable attention vector, $\|$ represents the splicing operation, N_i denotes the neighbor set of node i, and σ is the nonlinear activation function. To reduce computational complexity, this study employs a sparse graph construction strategy, retaining only directed edges within an $8D$ radius downstream of the wind direction projection, where D is the wind turbine diameter; this truncation radius remains consistent across all experiments. The GAT employs four attention heads, each with 128 hidden dimensions. After stacking three GAT layers, it outputs node-level feature vectors as shown in Figure 3. These node-level features are then global average-pooled to generate wind farm-level embeddings, which serve as the state input for the downstream reinforcement learning agent.

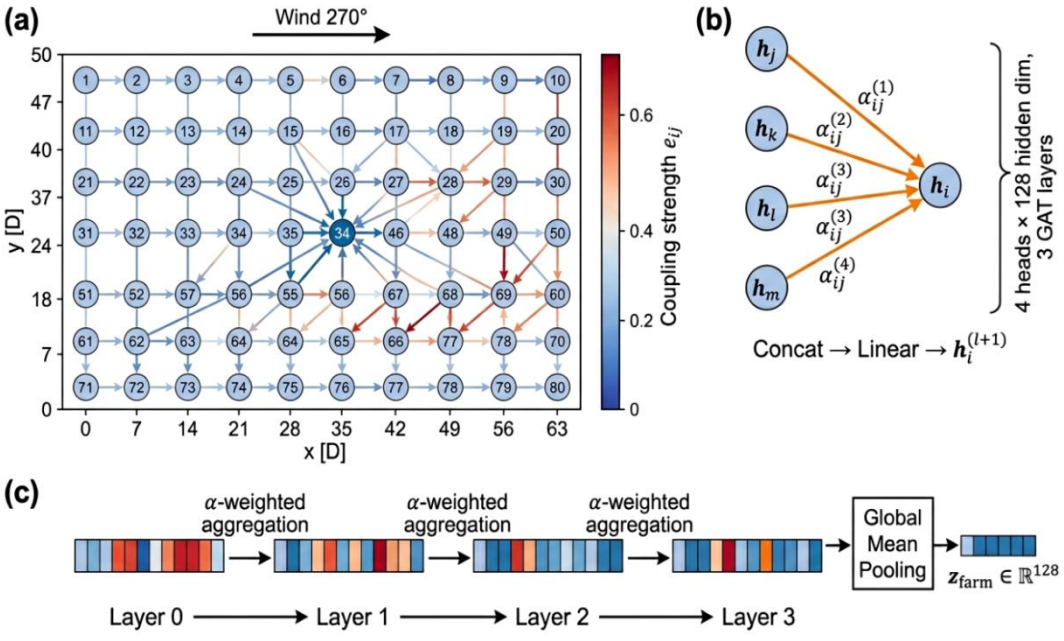


Figure 3 GAT multi-machine coupling characterization diagram

3.4 Deep Reinforcement Learning-Driven Layout Intelligent Optimization Algorithm

The layout optimization problem is formalized as a finite-time Markov decision process, with the five-tuple defined as shown in Equation (9). The state S represents the concatenation of the wind farm's global graph embedding provided by GAT and the current layout; the action A is a discrete adjustment vector for each turbine position, taking values $-D, 0, +D$ in the east, west, south,

and north directions; the state transition P is determined jointly by the layout update and the new flow field generated by the PINN agent; the reward r is a weighted sum of multiple objectives including power generation, wake uniformity, and engineering constraints; the discount factor $\gamma = 0.99$. The specific form of the multi-objective reward is given in Equation (10).

$$\mathrm{M} = \langle \mathrm{S}, \mathrm{A}, P, r, \gamma \rangle \tag{9}$$

$$r_t = w_1 \Delta \mathrm{AEP}_t - w_2 \sigma_{\mathrm{wake},t} - w_3 \mathrm{I}_{\mathrm{constraint},t} \tag{10}$$

In equation (10): $\Delta \mathrm{AEP}_t$ represents the percentage improvement in power generation relative to the baseline; $\sigma_{\mathrm{wake},t}$ denotes the variance of multi-unit wake intensity (to encourage uniformity); $\mathrm{I}_{\mathrm{constraint},t}$ is a penalty indicator variable for engineering constraints (unit spacing, boundary restrictions); and w_1, w_2, w_3 are relative weights set to $1.0 : 0.3 : 0.5$ after hyperparameter sensitivity analysis. Strategy training employs PPO, sharing parameters between the policy network and the value network, as shown in Figure 4. Both networks adopt a symmetric two-layer MLP architecture, illustrated in Figure 5. The PPO truncation objective limits policy updates within the confidence interval, as specified in equation (11).

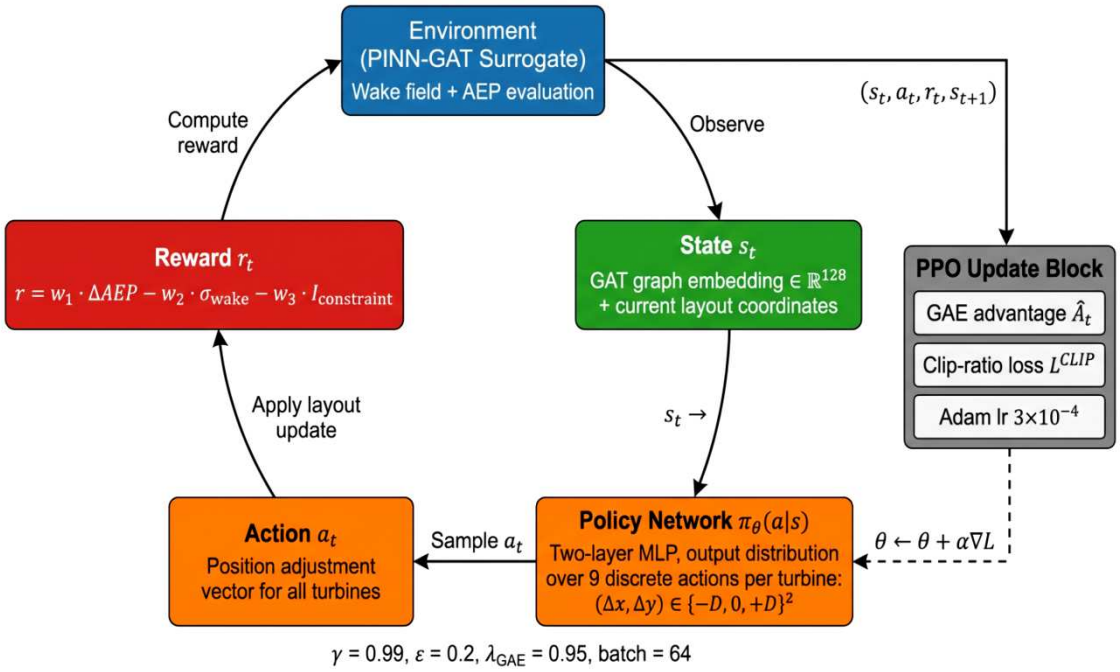


Figure 4 flow chart of intensive learning training

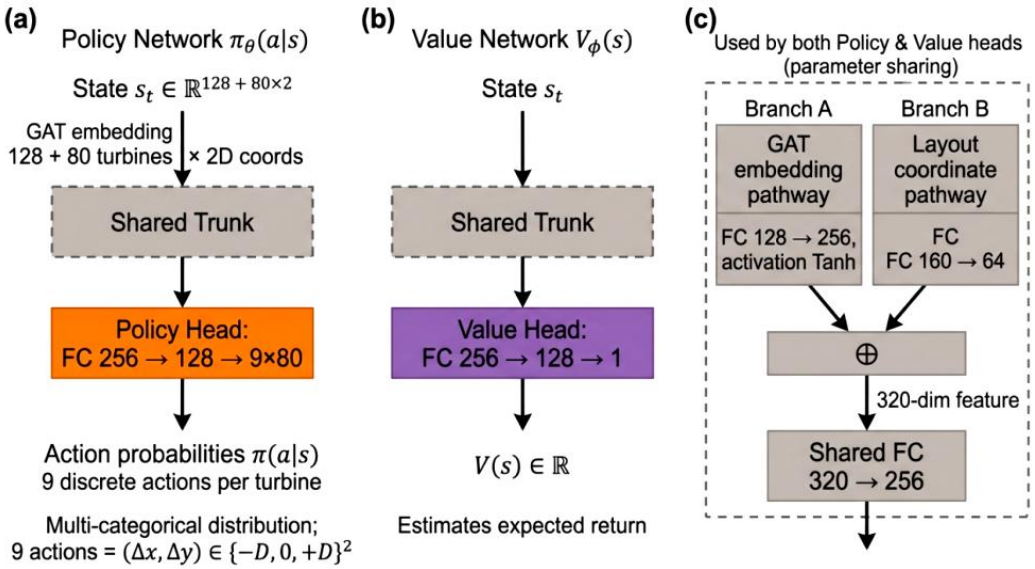


Figure 5 Schematic diagram of the PPO dual-network architecture

$$\mathscr{L}^{CLIP}(\theta)=E_t\left[\min\left(\rho_t(\theta)\hat{A}_t, clip(\rho_t(\theta),1-\epsilon,1+\epsilon)\hat{A}_t\right)\right] \tag{11}$$

In Equation 11, $\rho_t(\theta)=\pi_\theta(a_t|s_t)/\pi_{\theta_{old}}(a_t|s_t)$ represents the probability ratio of the new and old policies, $\hat{A}_t$ is the estimated advantage function (calculated using GAE), and $\grave{o}=0.2$ is the truncation threshold. The three-layer architecture achieves end-to-end coordination through a two-stage training approach: In the first stage, PINN and the GAT encoder are jointly trained on LES data to optimize L_{total} and ensure agent convergence; in the second stage, the PINN-GAT parameters are fixed while the PPO algorithm searches for the optimal policy layout, with action distributions updated via policy gradient backpropagation. The end-to-end coordination between the two training stages is illustrated in Figure 6. Key hyperparameters for the full training process are listed in Table 1.

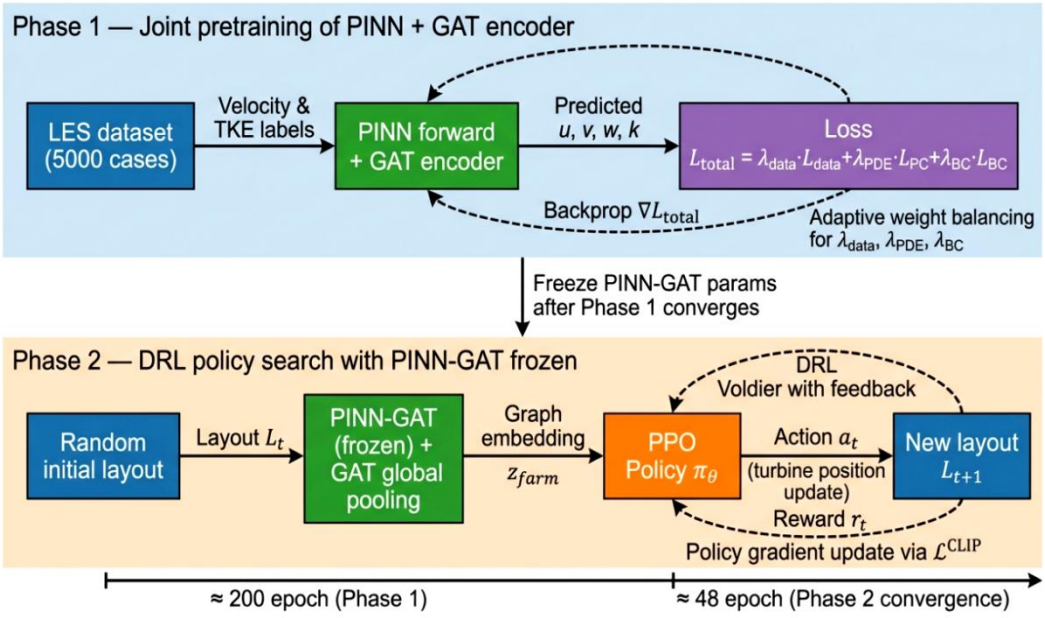


Figure 6 End-to-end collaborative training data flow diagram

Table 1 Key Hyperparameter Configuration of the PINN-GAT-DRL Framework

Module	Hyperparameter	Value
PINN	Hidden layers / dimensions	8 / 256
PINN	Activation function	SiLU
PINN	PDE collocation sampling points	5000
PINN	Loss term weights	Adaptive balancing
GAT	Attention heads / hidden dimensions	4 / 128
GAT	Number of GAT layers	3
GAT	Neighbor screening radius	8_D downstream of wind direction
DRL	PPO clipping threshold ϵ	0.2
DRL	Discount factor γ	0.99
DRL	GAE λ	0.95
DRL	Adam learning rate	3×10^{-4}
DRL	Reward weights $w_1:w_2:w_3$	1.0 : 0.3 : 0.5
Training	Pre-training / fine-tuning epoch limit	200 / 500 (converges at ~48 epochs in practice)
Training	Batch size	64

The hyperparameter values listed in Table 1 balance network capacity, training stability, and computational cost. The classic default parameters for PPO, $\gamma = 0.99$ and $\grave{o} = 0.2$, remain applicable within the discrete combinatorial space of wind farm layout [31]. The number of heads and hidden dimensions in GAT's multi-head attention mechanism were fine-tuned based on the sparsity of wind farm graph structures [32]. Although the upper epoch limit was set to 500 for safety redundancy during fine-tuning, the training curve shows that the policy reward typically plateaus around the 48th epoch, with actual training costs significantly lower than the upper limit.

4 Experimental Results

4.1 Data Set Construction and Experimental Environment Configuration

The experimental dataset utilizes a wake field sample library generated through LES simulation, referencing the geometric configurations of Horns Rev I and Lillgrund, with the NREL 5 MW wind turbine as the individual model. The turbine features a diameter of $D = 126$ m, hub height of 90 m, and a rated thrust coefficient of $C_T = 0.8$. It should be noted that this configuration represents a synthetic simulation scenario based on "Horns Rev I geometric topology + NREL 5 MW standardized model," rather than actual Horns Rev I measurement data, aiming to compare the performance of the method chain under a unified model. The computational domain is a rectangular prism measuring $20D \times 12D \times 10D$, with grid resolution refined to $D/24$ in the wake core region. Inlet wind velocities span 15 levels ranging from 4 to 25 m/s, while wind directions are sampled at 30-degree intervals across 12 sectors, covering the full operational spectrum from inlet to outlet wind speeds.

The layout samples include three types: regular arrays, staggered arrays, and irregular arrays, with turbine quantities varying from 30 to 200, yielding a total of 5,000 LES samples representing different operational layout combinations. These samples are divided into training, validation, and testing sets at ratios of 70%/15%/15%. The computing environment consisted of an NVIDIA A100 GPU cluster with eight cards performing parallel training, utilizing the PyTorch 2.1 and PyTorch Geometric deep learning frameworks. The operational conditions and typical layouts of the datasets are illustrated in Figure 7.

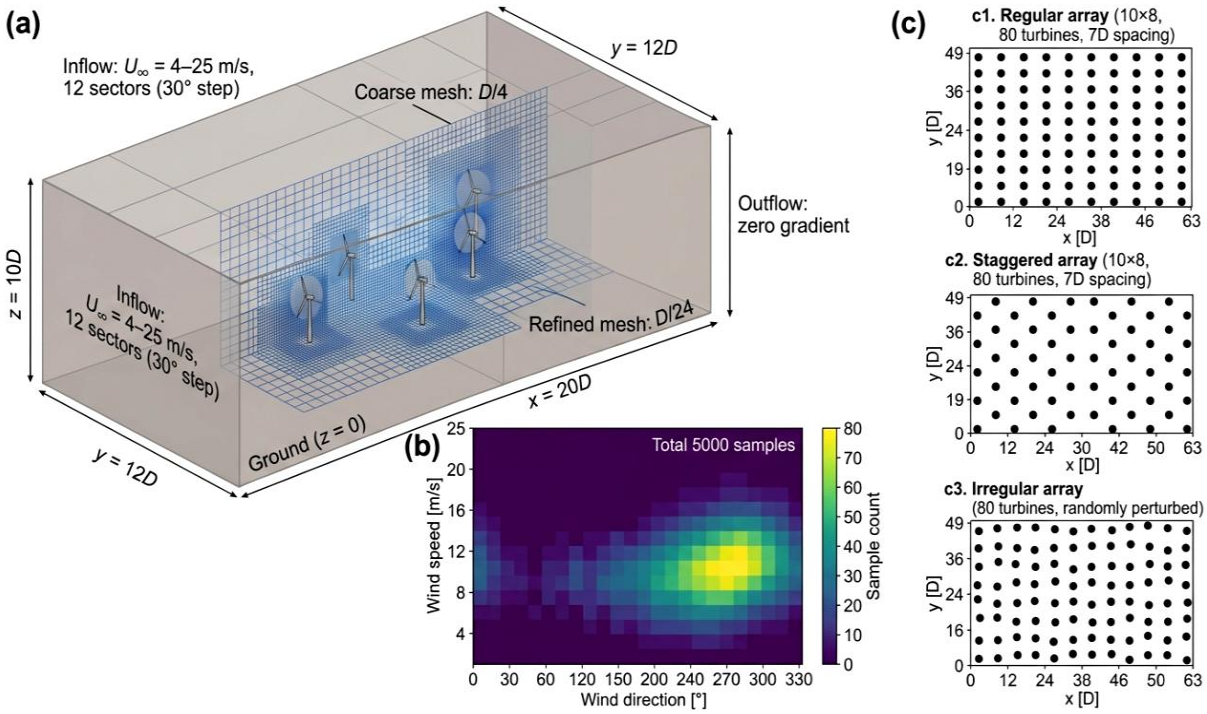


Figure 7 Schema of dataset construction

As shown in Figure 7, the operating conditions cover a higher density in the medium wind speed (8-12 m/s) and the typical dominant wind direction, which is consistent with the statistical distribution of real wind resources in the North Sea. The three types of typical layouts give consideration to both regular and irregular layouts common in practical engineering, ensuring the generalization training of the model in different layout forms. The data set size and division are shown in Table 2. As shown in Table 2, the training set accounts for 70%, the verification set and the test set account for 15% respectively. The samples are evenly sampled in the three-dimensional space of wind speed, wind direction and layout shape, avoiding over fitting under local conditions.

Table 2 Dataset Scale and Partition

Data Subset	Sample Size	Operating Condition–Layout Proportion	Wind Speed Range (m/s)	Wind Direction Sectors
Training set	3500	70%	4–25	12
Validation set	750	15%	4–25	12
Test set	750	15%	4–25	12
Total	5000	100%	—	—

4.2 Evaluation of prediction accuracy and calculation efficiency of wake field

Four baselines are set for the accuracy comparison of the proxy model: Jensen analytical wake model, bastankhah port é -agel Gaussian model, CNN only data-driven model (without physical constraints), and the pinn-gat coupling proxy in this study. Les simulation results are taken as true values, and the time average velocity field is compared point by point on 750 working conditions of the test set. The comparison between the wake field of single machine and the wake field of 8-machine array is shown in Figure 8.

As shown in Figure 8, the Jensen model abstracts the wake as a top hat shaped velocity loss, and the deep wake area is significantly underestimated; The bastankhah Gauss model restores the Gauss defect contour, but the error accumulates in the superposition area of multiple machines; The accuracy of CNN only in the shallow wake region is acceptable, but there is a "pseudo steady state" drift in the far wake (outside the downstream 8D); Because pinn-gat takes N-S residuals and

continuity equation residuals as soft constraints, the flow field still obeys the conservation law in the data sparse area, and the maximum deviation from the truth of LES is controlled within 7%. The centerline velocity profile further shows that pinn-gat is close to Les curve in the whole 2d-12d process. The quantitative comparison of prediction accuracy is shown in Table 3.

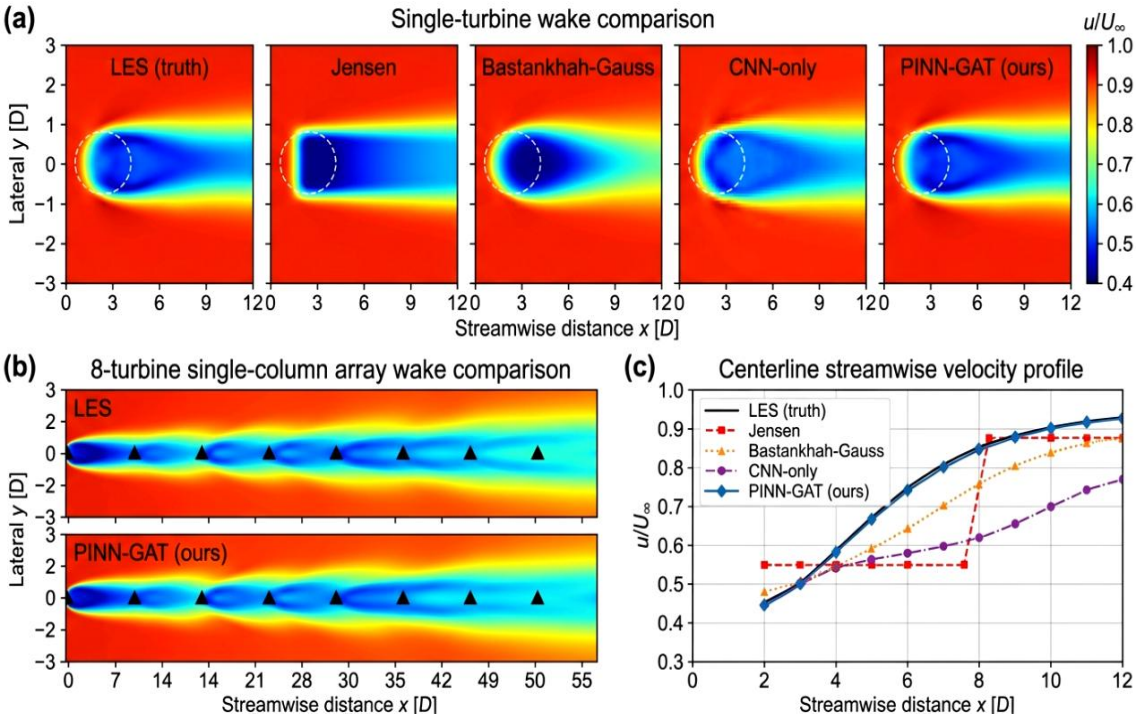


Figure 8 Comparison and combination diagram of prediction accuracy of wake flow field

Table 3 Quantitative Comparison of Wake Field Prediction Accuracy and Computational Efficiency

Model	RMSE (m/s)	MAE (m/s)	R^2	Single-Condition Inference Time
LES (ground truth)	—	—	—	3.8 h
Jensen model	0.94	0.71	0.83	< 1 ms
Bastankhah-Gauss	0.66	0.48	0.89	5 ms
CNN-only	0.43	0.31	0.93	28 ms
PINN-GAT (this study)	0.22	0.16	0.97	41 ms

As shown in Table 3, the PINN-GAT proposed in this study achieves a 67% reduction in RMSE compared to Bastankhah-Gauss and a 49% improvement over CNN-only; its R^2 increases from 0.93 for CNN-only to 0.97, approaching the accuracy of LES. In terms of computational efficiency, PINN-GAT maintains a single-condition inference time of approximately 41 ms, representing an acceleration of about 3.3×10^5 times compared to LES's 3.8 hours, fully meeting the real-time requirements for thousands of evaluations in layout optimization. The statistical comparison between prediction error distributions and computational efficiencies of the methods is presented in Figure 9.

As shown in Figure 9, the residual distribution of pinn-gat is narrower and more symmetrical, and the median is close to the zero line; Under different wind speed ranges, such as cut in wind speed range (4-7 M/s) and rated wind speed range (11-15 M/s), the fluctuation range of RMSE is only 0.04-0.06 M/s, showing robustness to changes in working conditions. The logarithmic scatter plot of calculation time accuracy reveals that this method is in the lower right quadrant of "high accuracy+sub second level", which is neither as time-consuming as Les nor as precision limited as Jensen.

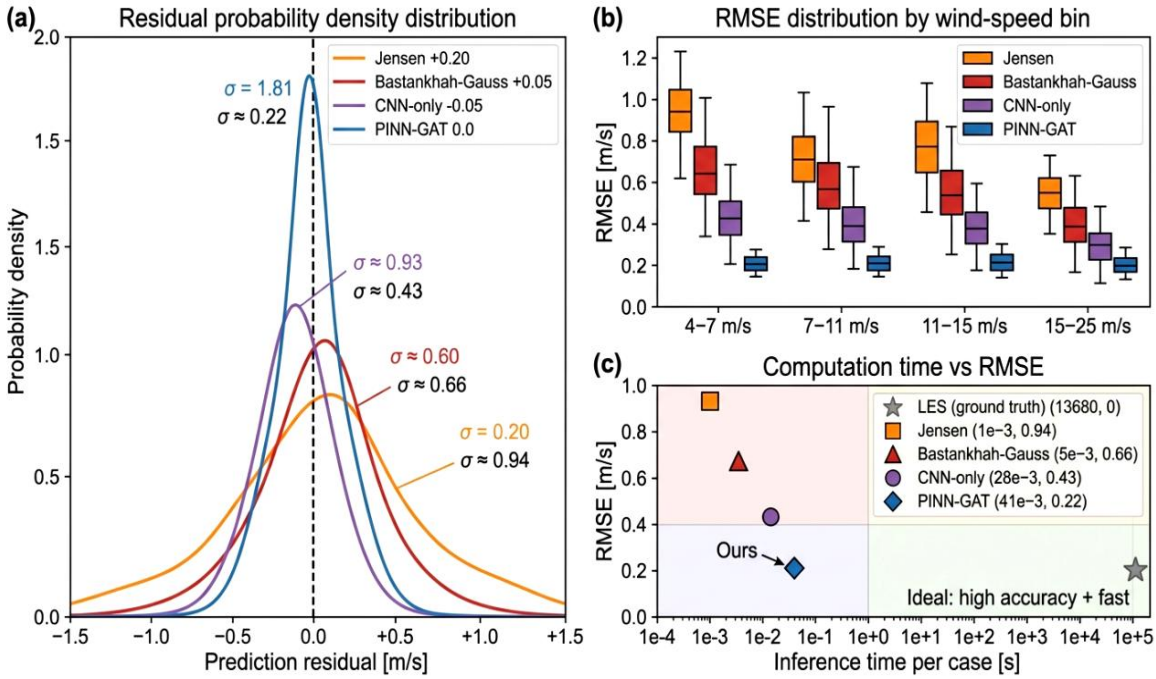


Figure 9 Combined statistical chart of prediction error distribution and computational efficiency

4.3 Comparison of layout optimization results and benchmark methods

The layout optimization is carried out on the benchmark site with the same scale of horns Rev I (80 fans, 10×8 array, and the fan spacing is about $7\,D$), and the optimization goal is to maximize the annual power generation and reduce the wake loss. Four groups of benchmark algorithms are selected: Ga+Jensen, PSO+bastankhah Gauss, Bo+CNN only, and DRL+pinn-gat in this study. The comparison between the cumulative reward curve of optimization training and the convergence behavior of each algorithm is shown in Figure 10.

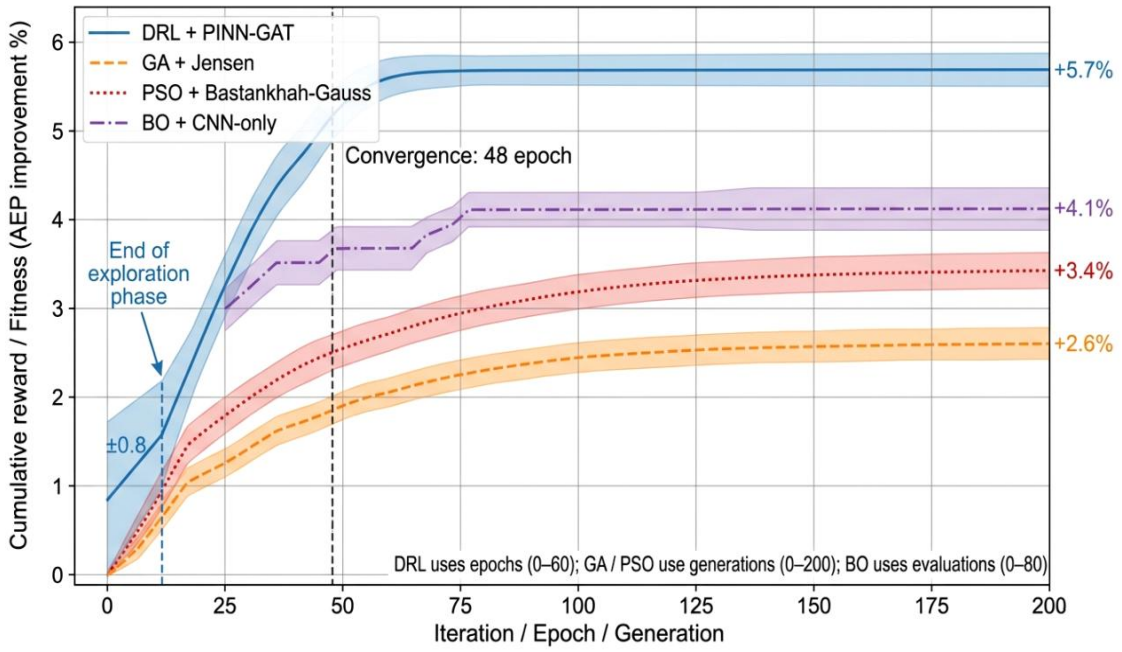


Figure 10 Comparison of convergence and algorithm performance in layout optimization training

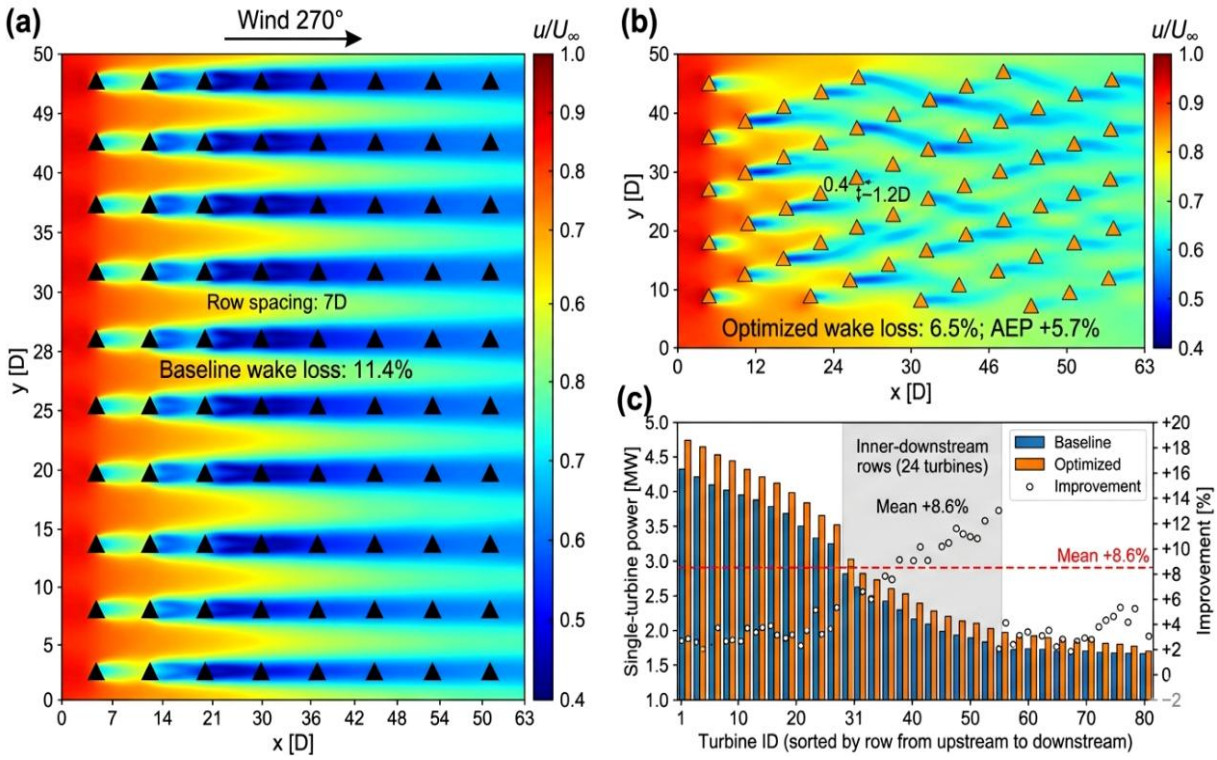


Figure 11 compares the layout before and after optimization and the power distribution of individual units

As shown in Figure 11, the optimized layout offsets rows of fans with opposing wind directions by 0.4–1.2 D along the dominant wind direction, reducing the lateral spacing to 6 D and increasing the longitudinal spacing to 8 D, resulting in a significant reduction in the wake overlap area along the dominant wind direction. The single-unit power of downstream inner rows of fans showed the most notable improvement: Figure 11(c) indicates that the average power of the 24 inner rows most affected by wake effects under the baseline increased by 8.6% after layout adjustment, demonstrating that the optimization redirected more wind resources to positions previously most susceptible to wake suppression. Quantitative comparisons of the layout optimization effects are presented in Table 4.

Table 4 Layout Optimization Results and Algorithm Comparison (80-Turbine Benchmark Field)

Optimization Framework	AEP Improvement	Wake Loss	Convergence Iterations	Algorithm Runtime
Baseline (regular array)	—	11.40%	—	—
GA + Jensen	2.60%	9.10%	200 generations	18.4 h
PSO + Bastankhah-Gauss	3.40%	8.40%	180 generations	22.1 h
BO + CNN-only	4.10%	7.60%	80 evaluations	26.7 h
DRL + PINN-GAT (this study)	5.70%	6.50%	48 epochs	31.3 h

As shown in Table 4, the AEP improvement of this research framework is 3.1% higher than GA+Jensen, 2.3% higher than PSO+bastankhah Gauss, and 1.6% higher than Bo+CNN only; The wake loss decreased from 11.4% of baseline to 6.5%, a decrease of 4.9%. The running time of the algorithm is slightly higher than the benchmark, but it is still within the acceptable range of engineering, and the convergent epoch number is significantly less than the algebra of the heuristic algorithm. The multi-objective Pareto front is shown in Figure 12.

As shown in Figure 12, the Pareto front given by DRL+pinn-gat "envelops" the front of three sets of benchmark methods in two target dimensions, that is, higher power generation can be achieved under the same wake uniformity, and better wake uniformity can be achieved under the

same wake uniformity. This two-dimensional synchronous improvement is difficult for a single objective heuristic algorithm to take into account.

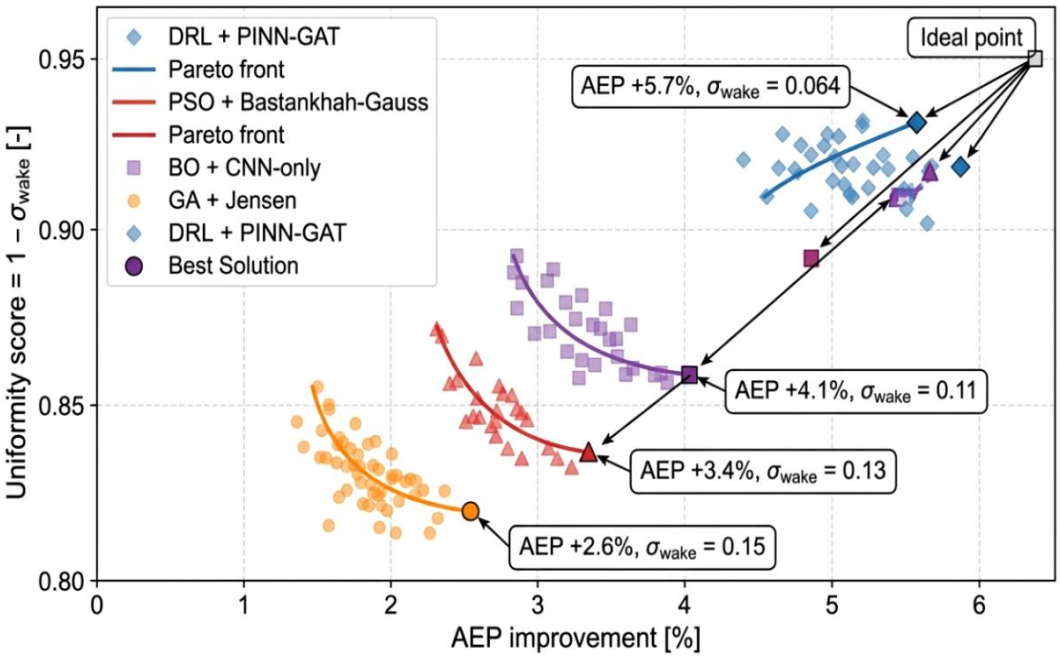


Figure 12 Comparison of multi-objective Pareto frontiers and algorithms

4.4 Robustness and scalability analysis under wind disturbance

The test set is divided into five categories according to the complexity of wind conditions (homogeneous wind, bidirectional wind, multidirectional wind, high turbulence intensity, vertical shear). The AEP improvement under each type of wind condition is re counted, and the robustness results are shown in Table 5.

As shown in Table 5, this method achieves an AEP improvement ranging from 4.4% to 5.9% across five wind condition categories, with a maximum variation of 1.5 percentage points. The BO + CNN-only approach shows an AEP improvement dropping to 3.2% under high turbulence intensity, while PSO + Bastankhah-Gauss further decreases to 2.7%. This comparison demonstrates that physical information constraints significantly mitigate the accuracy degradation of purely data-driven models under complex turbulent conditions. Scalability tests covering five turbine configurations (30,50,80,120, and 200 units) are presented in Figure 13.

Table 5 Robustness Comparison of Layout Optimization Results Under Multiple Wind Conditions

Wind Condition Type	Dominant Wind Direction Proportion	Average TI	DRL+PINN-GAT Improvement	BO+CNN-only Improvement	PSO+Gauss Improvement
Homogeneous wind (single dominant)	78%	0.07	5.90%	4.30%	3.60%
Bidirectional wind (two dominant)	56% / 32%	0.09	4.80%	3.70%	3.20%
Multidirectional wind (12 sectors)	Uniform	0.1	5.30%	3.90%	3.10%
High turbulence intensity	—	0.16	4.40%	3.20%	2.70%
Strong vertical shear	—	0.08	4.70%	3.40%	2.90%

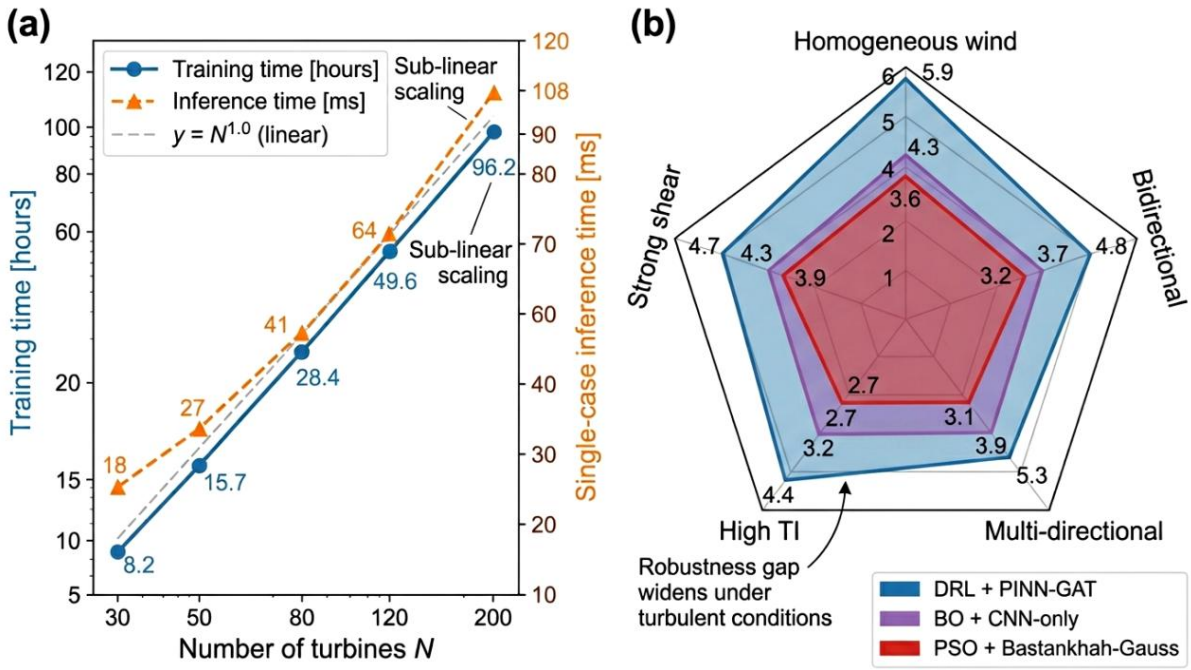


Figure 13 Combined diagram of scalability and robustness under diverse wind conditions for wind farms of different scales

As shown in Figure 13, the training duration increases approximately linearly with the number of fans. The complete training takes about 96 hours under the scale of 200 units, while the standard pole field of 80 units is 28.4 hours. The expansion coefficient is far less than the quadratic term growth of the heuristic algorithm. The increase of AEP was stable at 5.2% -5.7% in the range of 30-120 units, and fell back to 4.8% in the super large scale range of 200 units. The main reason is that the neighbor screening radius of attention needs further fine adjustment in the super large field. Radar polygon display this method constitutes the "outer envelope" of the reference method under five types of wind conditions, and the robustness advantage is more significant with the increase of wind complexity. The scalability indicators are shown in Table 6.

As shown in Table 6, the reasoning time expands approximately linearly with the number of fans, and remains at the order of 100 milliseconds under the scale of 200 units, which is far below the time-consuming threshold of real-time call of the project; The growth of memory consumption is moderate, and there is still sufficient margin within the range of 80 GB video memory of A100 single card, which has the potential to further expand to 1000 super large fields.

Table 6 Scalability Indicators for Wind Farms of Different Scales

Number of Turbines	Training Duration	Inference Time (single condition)	AEP Improvement	Memory Usage
30	8.2 h	18 ms	5.20%	6.4 GB
50	15.7 h	27 ms	5.50%	9.8 GB
80	28.4 h	41 ms	5.70%	14.2 GB
120	49.6 h	64 ms	5.40%	19.1 GB
200	96.2 h	108 ms	4.80%	28.6 GB

5 Discussion

5.1 Key results discussion and mechanism analysis

The experimental results show that the accuracy, efficiency and robustness of the three-tier coupling framework have been significantly improved synchronously, which is not accidental. From

the perspective of accuracy, pinn writes the RANS residuals into the loss function in the form of soft constraints, which is equivalent to forcing the network to obey the conservation law in the data sparse area. This is an inductive bias that CNN only and other pure data-driven models cannot obtain from the architecture. The bastankhah Gauss model is limited by Gauss profile and linear superposition assumption, and the accuracy degradation in the far wake region and multi machine coupling region is inevitable; Even if the data-driven CNN is trained on the fine grid, the non physical output will still appear due to the lack of physical consistency when extrapolating to unfamiliar working conditions. This exactly corresponds to the general dilemma of the precision gap between high fidelity models and lightweight agents pointed out by Houck in the wake management review [33]. Gat regards each fan as a graph node, encodes the upstream and downstream coupling into a directed edge, and explicitly incorporates the spatial structure into the internal representation of the network, which is fundamentally different from the existing data-driven wake model, which discards the superposition of multiple fans to post-processing.

From the perspective of efficiency and robustness, the advantages of DRL alternative heuristic algorithm are particularly prominent in windy conditions. Heuristic algorithms such as GA and PSO are robust under low dimensional or single working conditions, but the rise of dimension and the complexity of wind conditions will make the search fall into local optimum; PPO's strategy level search model "layout generation" as sequential decision-making, and the exploration of solutions in high-dimensional space is more directional. In Table 5, this method can still maintain an AEP increase of 4%-5% under high turbulence and shear wind conditions, which is in contrast to the decline of the benchmark method. The core source of this difference in robustness is the physical consistent flow field provided by the pinn agent under complex turbulent conditions, which raises the accuracy ceiling of the "Environment Simulator" to a level that can not be reached by simple heuristics. The summary of the discussion results is shown in Table 7.

As shown in Table 7, improvements across all five dimensions correspond to specific design choices within the framework, offering strong interpretability and facilitating module-level fault localization and fine-tuning at the engineering site.

Table 7 Key Results and Corresponding Mechanisms

Result Dimension	Quantitative Improvement	Primary Mechanism
Flow field prediction RMSE	67% lower than Gauss	RANS residual soft constraint + GAT multi-turbine coupling
Single-condition inference speed	3.3×10^5 times faster than LES	Neural network forward pass + shared encoding backbone
AEP improvement	1.6 pp higher than BO+CNN	DRL policy-level search + end-to-end collaboration
Multi-wind-condition robustness	Range of 1.5 pp	PINN surrogate maintains accuracy under complex conditions
Scalability	200 turbines with approximately linear time growth	Graph sparsification + adaptive neighbor screening radius

5.2 Calculation efficiency and project deployment value

The sub second single condition reasoning is the key threshold for embedding the agent model into the full cycle decision-making of "wind farm layout grid connection dispatching". This method compresses the reasoning to 41 MS in 80 standard pole fields, and still maintains the 108 ms level in 200 super large fields, which can be called in real time under the conventional calculation conditions of the project site. This speed level enables layout optimization to enter the "online rolling" mode: rapidly produce multiple candidate schemes at the initial stage of site selection, and adjust and evaluate when the wind resource data is updated, instead of starting CFD simulation for several hours each time. Bempedelis et al. Pointed out that data-driven agent combined with Les high fidelity data is "a feasible path for future wind farm design" [6]. The empirical results of this method provide further support for this judgment in terms of accuracy speed.

At the level of system deployment, the engineering significance of increasing AEP by 5.7%

should not be underestimated. Based on the 400 MW installed capacity of 80 5 MW wind turbines, the annual utilization hours of 3500 h, and the on grid electricity price of 0.5 yuan/kwh, the 5.7% increase in AEP corresponds to an annual income increase of about 40million yuan; According to the 25 year life cycle, the cumulative economic value is nearly 1billion yuan. This figure only comes from the layout optimization itself, and does not superimpose the further gain brought by the active wake control during operation. The multi-objective Pareto frontier reveals the trade-off space of "power generation wake uniformity". The engineering party can select a compromise point on the frontier curve according to the constraints of power grid accommodation capacity and unit fatigue life budget, and truly change the layout optimization from "Post Examination" to "pre design".

5.3 Analysis of research limitations

The limitations of this study can be summarized into two dimensions. On the one hand, Les training data is still generated by RANS simulation. The long-term observation data of SCADA and lidar in the real site are not deeply integrated into the training cycle. The generalization ability of the proxy model under real conditions such as extreme weather, complex terrain, and machine sea interaction remains to be verified by large-scale tests. Previous studies have generally pointed out that the turbulence intensity, vertical shear and atmospheric stability of the real site have a significant impact on the wake recovery, and the next work should promote the fine-tuning and online learning of the pinn agent on the real SCADA data. On the other hand, the training cost of DRL strategy is still higher than that of simple heuristics. The complete training takes nearly 100 hours under the scale of 200 sets. Although it is acceptable in the engineering time scale, it still lags behind the demand for immediate deployment. In the future, we can explore the combination strategy of meta learning and course learning, and transfer the strategy between multiple venues to amortize the training cost, so as to make the framework evolve in the direction of real "plug and play".

6 Summary

Aiming at the core technical problem of wind farm wake loss, which has long plagued the large-scale expansion of wind power, this study constructed an end-to-end collaborative framework of "pinn physical consistent wake agent+gat multi machine coupling characterization+DRL strategy level layout optimization", which promoted the integration of deep learning and fluid dynamics from a single point agent to a system level closed loop. The main work and contributions are summarized as follows:

(1) Surrogate model of wake field constrained by physical information. Taking the residuals of RANS momentum equation and continuity equation as the soft constraint embedding loss function, RMSE is 67% lower than that of bastankhah Gauss model, 49% lower than that of CNN only, and R^2 is increased to 0.97 in the comparison of Les truth value, maintaining physical consistency in the data sparse area and far wake area.

(2) Multi aircraft wake coupling representation based on graph attention network. Each fan is regarded as a graph node, and the upstream and downstream coupling under the wind direction projection is coded as a directed edge feature. By learning the coupling weight with multiple heads' attention, the limitations of the existing GNN model relying on the predefined adjacency matrix and insufficient attention mechanism are overcome, providing a compact and spatially aware intermediate representation for the downstream optimizer.

(3) An intelligent layout optimization algorithm driven by deep reinforcement learning. The layout selection is formalized as MDP, and PPO training is driven by multi-objective weighted rewards of power generation, wake uniformity and engineering constraints. On the benchmark field of horns Rev I with the same scale (80 fans), the AEP increased by 5.7%, and the wake loss

decreased from 11.4% of baseline to 6.5%, maintaining a stable improvement of 4.4% -5.9% under five types of wind conditions.

(4) End to end collaboration and engineering deployment capabilities. The three-layer module realizes end-to-end cooperation through two-stage training, and the single condition reasoning is 41 MS, and 200 super large fields are 108 MS, which can be called in real time at the project site. The multi-objective Pareto front envelops three sets of benchmark methods, providing a controllable trade-off space for the engineering party to "generate electricity - Wake uniformity".

There is still room for improvement in the two directions of deep integration of real site observation data and further compression of DRL training cost. The follow-up work will focus on issues such as real SCADA data fine-tuning, meta learning course learning joint training, and multi site strategy migration.

Author contributions

Shujie Liu and Shengqiao Chen: Conceptualization, Methodology, Data curation, Formal analysis, Visualization, Writing—original draft, Writing—review and editing; **Bo Xiang**: Supervision, Project administration, Data Curation, Validation, Writing—original draft, Writing—review and editing.

Funding

This research did not receive any specific grant from funding agencies in the public, commercial, or not-for-profit sectors.

Declaration of Interest

The authors declared no potential conflicts of interest with respect to the research, authorship, and/or publication of this research article.

Data availability

The original data of this study can be obtained from the corresponding author.

References

[1] Magar V, Peña A, Hahmann A N, Pacheco-Rojas D A, García-Hernández L S, Gross M S. Wind energy and the energy transition: Challenges and opportunities for Mexico. Sustainability, 2023, 15(6): 5496.

[2] Yang K, Zhang M, Yang S, Song Y, Dong X, Deng Y, Deng X. Pareto frontier for multi-objective wind farm layout optimization balancing power production and turbine fatigue life. Renewable Energy, 2025, 252: 122987.

[3] Li B, Ge M, Li X, Liu Y. A physics-guided machine learning framework for real-time dynamic wake prediction of wind turbines. Physics of Fluids, 2024, 36(3): 035143.

[4] Yang K, Deng X, Ti Z, Yang S, Huang S, Wang Y. A data-driven layout optimization framework of large-scale wind farms based on machine learning. Renewable Energy, 2023, 218: 119290.

[5] Wang Q, Ti Z, Yang S, Yang K, Wang J, Deng X. Hierarchical dynamic wake modeling of wind turbine based on physics-informed generative deep learning. Applied Energy, 2025, 378: 124812.

[6] Bempedelis N, Magri L, Steiros K. Data-driven optimisation of wind farm layout and wake steering with large-eddy simulations. Wind Energy Science, 2024, 9(4): 869-882.

[7] Kim T, Kim C, Song J, You D. Optimal control of a wind farm in time-varying wind using deep reinforcement learning. Energy, 2024, 303: 131841.

[8] Ling Z, Zhao Z, Liu Y, Liu H, Ali K, Liu Y, Wen Y, Wang D, Li S, Su C. Multi-objective layout optimization for wind farms based on non-uniformly distributed turbulence and a new three-dimensional multiple wake model. Renewable Energy, 2024, 227: 120558.

[9] Bastankhah M, Porté-Agel F. A new analytical model for wind-turbine wakes. Renewable Energy, 2014, 70: 116-123.

[10] Yousif M Z, Yu L, Lim H. Physics-guided deep learning for generating turbulent inflow conditions. Journal of Fluid Mechanics, 2022, 936: A21.

[11] Duthé G, Abdallah I, Barber S, Chatzi E. Flexible multi-fidelity framework for load estimation of wind farms through graph neural networks and transfer learning. Data-Centric Engineering, 2024, 5: e30.

[12] Kim H, Kim J, Won S, Lee C. Unsupervised deep learning for super-resolution reconstruction of turbulence. Journal of Fluid Mechanics, 2021, 910: A29.

[13] Wang L, Dong M, Yang J, Wang L, Chen S, Duić N, Joo Y H, Song D. Wind turbine wakes modeling and applications: Past, present, and future. Ocean Engineering, 2024, 309: 118508.

[14] van der Laan M P, Kelly M, Baungaard M, Dicholkar A, Hodgson E L. A simple steady-state inflow model of the neutral and stable atmospheric boundary layer applied to wind turbine wake simulations. Wind Energy Science, 2024, 9(10): 1985-2000.

[15] Santoni C, Zhang D, Zhang Z, Samaras D, Sotiropoulos F, Khosronejad A. Toward ultra-efficient high-fidelity predictions of wind turbine wakes: Augmenting the accuracy of engineering models with machine learning. Physics of Fluids, 2024, 36(6): 065159.

[16] Faroughi S A, Pawar N M, Fernandes C, et al. Physics-guided, physics-informed, and

physics-encoded neural networks and operators in scientific computing: Fluid and solid mechanics. ASME Journal of Computing and Information Science in Engineering, 2024, 24(4): 040802.

[17] Cai S, Mao Z, Wang Z, Yin M, Karniadakis G E. Physics-informed neural networks (PINNs) for fluid mechanics: A review. Acta Mechanica Sinica, 2021, 37(12): 1727-1738.

[18] Cuomo S, Di Cola V S, Giampaolo F, Rozza G, Raissi M, Piccialli F. Scientific machine learning through physics-informed neural networks: Where we are and what's next. Journal of Scientific Computing, 2022, 92(3): 88.

[19] Renganathan S A, Maulik R, Letizia S, Iungo G V. Data-driven wind turbine wake modeling via probabilistic machine learning. Neural Computing and Applications, 2022, 34(8): 6171-6186.

[20] Ye M, Li M, Liu M, Wan D, Chen H C. Overview of data-driven models for wind turbine wake flows. Journal of Marine Science and Application, 2025, 24(1): 1-20.

[21] Liu X, Zhang Y, Zhen Z, Xu F, Wang F, Mi Z. Spatio-temporal graph neural network and pattern prediction based ultra-short-term power forecasting of wind farm cluster. IEEE Transactions on Industry Applications, 2024, 60(1): 1–15.

[22] Peng X, Li Y, Tsung F. A graph attention network with spatio-temporal wind propagation graph for wind power ramp events prediction. Renewable Energy, 2024, 236: 121280.

[23] Romero D A, Hasanpoor S, Antonini E G A, Amon C H. Predicting wind farm wake losses with deep convolutional hierarchical encoder-decoder neural networks. APL Machine Learning, 2024, 2(1): 016111.

[24] Song M, Huang J, Shao X, Zhao S, Ma C, Qi Z. A three-dimensional dynamic wake prediction framework for multiple turbine operating states based on diffusion model. Energy, 2025, 333: 137523.

[25] Bouchekara H R E H, Ramli M A M, Javaid M S. Wind farm layout optimization/expansion of real wind turbines with a parallel collaborative multi-objective optimization algorithm. Energies, 2024, 17(22): 5601.

[26] Malisani P, Bartement T, Bozonnet P. Offshore wind farm layout optimization with alignment constraints. Wind Energy Science, 2025, 10(8): 1611-1623.

[27] Liew J, Göçmen T, Lio W H, Larsen G C. Model-free closed-loop wind farm control using reinforcement learning with recursive least squares. Wind Energy, 2024, 27(11): 1109-1124.

[28] Yu X, Lu Y. Reinforcement learning-based multi-objective differential evolution for wind farm layout optimization. Energy, 2023, 284: 129300.

[29]Hu W, Yang Q, Yuan Z, Yang F. Wind farm layout optimization in complex terrain based on CFD and IGA-PSO. Energy, 2024, 288: 129907.

[30] Bizon Monroc C, Bušić A, Dubuc D, Zhu J. WFCRL: A multi-agent reinforcement learning benchmark for wind farm control[C]. Proceedings of the 38th Conference on Neural Information Processing Systems (NeurIPS 2024) Datasets and Benchmarks Track, 2024. arXiv:2501.13592.

[31] Karniadakis G E, Kevrekidis I G, Lu L, Perdikaris P, Wang S, Yang L. Physics-informed machine learning. Nature Reviews Physics, 2021, 3: 422-440.

[32] Wu Z, Pan S, Chen F, Long G, Zhang C, Yu P S. A comprehensive survey on graph neural networks. IEEE Transactions on Neural Networks and Learning Systems, 2021, 32(1): 4-24.

[33] Houck D R. Review of wake management techniques for wind turbines. Wind Energy, 2022, 25(2): 195-220.